

# The temperature–flow renormalization group and the competition between superconductivity and ferromagnetism

Carsten Honerkamp<sup>1</sup> and Manfred Salmhofer<sup>2</sup>

<sup>1</sup> *Theoretische Physik, ETH-Hönggerberg, CH-8093 Zürich, Switzerland*

<sup>2</sup> *Theoretische Physik, Universität Leipzig, D-04109 Leipzig, Germany*

(May 10, 2001)

We derive a differential equation for the one–particle–irreducible vertex functions of interacting fermions as a function of the temperature. Formally, these equations correspond to a Wilsonian renormalization group (RG) scheme which uses the temperature as an explicit scale parameter. Our novel method allows us to analyze the competition between superconducting and various magnetic Fermi surface instabilities in the one–loop approximation. In particular this includes ferromagnetic fluctuations, which are difficult to treat on an equal footing in conventional Wilsonian momentum space techniques. Applying the scheme to the two-dimensional  $t$ - $t'$  Hubbard model we investigate the RG flow of the interactions at the van Hove filling with varying next-nearest neighbor hopping  $t'$ . Starting at  $t' = 0$  we describe the evolution of the flow to strong coupling from an antiferromagnetic nesting regime over a  $d$ -wave regime at moderate  $t'$  to a ferromagnetic region at larger absolute values of  $t'$ . Upon increasing the particle density in the latter regime the ferromagnetic tendencies are cut off and the leading instability occurs in the triplet superconducting pairing channel.

## I. INTRODUCTION

Wilsonian momentum shell renormalization group (RG) schemes have become an important tool for the weak-coupling analysis of interacting electron systems because they provide a means to sum competing classes of diagrams in perturbation theory in a consistent manner. Moreover, with the Wilsonian RG schemes one can systematically approach potential singularities, which would cause problems in a direct perturbation expansion. Successes of RG methods in interacting electron systems are for example clear arguments for the stability of the Landau-Fermi liquid in two and more spatial dimensions for short range repulsive interactions and non-nested Fermi surfaces unless a Kohn-Luttinger instability intervenes at lowest temperatures<sup>1–3</sup>, or the classification of ground states in quasi-one-dimensional systems<sup>4–6</sup>. Moreover, numerous one-loop RG calculations have been used recently to analyze the interplay between antiferromagnetic (AF) and  $d$ -wave superconducting (SC) pairing tendencies in the two-dimensional (2D) Hubbard model<sup>7–16</sup>. On the other hand, the Hubbard model was originally introduced to describe ferromagnetism (FM) of itinerant electrons (see, e.g., Refs. 17,18). The existence of spin-polarized ground states has been proven in one-dimensional<sup>18,19</sup> and in special higher-dimensional<sup>20</sup> models and also established in the limit of infinitely many dimensions<sup>21,22</sup>. In the  $t - t'$  Hubbard model on the 2D square lattice at weak to moderate  $U$ , Hartree–Fock results<sup>23</sup>,  $T$ -matrix approximation together with Quantum Montecarlo simulations<sup>24,25</sup> and a generalized random phase approximation approach including local particle-particle correlations<sup>26</sup> point towards a FM regime for larger absolute values of  $t'$  around the van Hove filling where the Fermi surface (FS) contains the saddle points at  $(\pm\pi, 0)$  and  $(0, \pm\pi)$ . Recent parquet calculations<sup>27</sup> indicated similar tendencies. However, momentum-shell RG methods have up to now not produced any evidence confirming these findings.

In this paper we introduce a novel RG scheme, which we call the temperature–flow RG. Its distinguishing feature is that the temperature itself plays the role of the flow parameter. Indeed, it has been observed in many studies that varying a cutoff scale is in many ways similar to varying the temperature, but here we provide an exact RG flow equation for the one–particle–irreducible correlation functions, parameterized by the temperature. Using this method, we show that in the one–loop approximation, one finds a ferromagnetic regime in the  $t - t'$  Hubbard model. More precisely, the new flow is similar to previous ones for small  $t'$  and near to half–filling, but for larger  $|t'|$ , a ferromagnetic regime appears. The boundary of the FM phase is roughly at the same  $t'_c$  where it would be in the Hartree–Fock approximation, but with our RG calculation we find a *quantum critical point* separating the FM regime from a  $d$ -wave superconducting regime instead of a first order transition to an AF phase as in Hartree–Fock. We also find a triplet superconducting state when the filling is increased above the van Hove value.

In the following, we discuss the reasons why this FM phase was not seen in previous RG calculations. The main point is that when the flow parameter is given by an infrared cutoff, the particle–hole excitations with small total momentum are artificially suppressed above the scale set by the temperature, but in many interesting cases one cannot

run the flow down to these low scales because the one-loop RG flow of the interactions leads to strong coupling and even diverges at a nonzero scale.

In RG flows to strong coupling, the main interest is to determine the nature of the strongly coupled state. Very often there are several candidates for the latter and it is natural to assume that the strong coupling state with the highest energy gain will be realized. In the RG treatment this state is typically associated with the dominant channel at the energy scale at which the RG flow diverges, e.g. determined through an analysis of the corresponding susceptibilities. However, one-loop flows become unreliable once the coupling constants get larger than a value which depends, among other factors, on the Fermi surface. Thus it can happen that the one-loop approximation breaks down before processes involving particle-hole fluctuations at small wave-vectors, which could drive ferromagnetism or screen longer-ranged interactions, can intervene. Because of its inequivalent treatment of FM fluctuations on the one side and AF and SC tendencies on the other side, this type of momentum shell RG with infrared cutoff does presumably not represent, at least when used too straightforwardly, an appropriate method to answer the question which of the channels prevails<sup>28</sup>.

Thus, although momentum shell schemes apply, and can even be controlled rigorously, as long as the running coupling constants do not get large, it is interesting to investigate and compare alternative schemes which are not based on strict infrared cutoffs and therefore capable of taking into account low-energy fluctuations at all wave-vectors in the same way.

We now specifically discuss the Stoner problem. Consider an electron system with a density of states  $\rho$  per spin orientation and a repulsive onsite interaction  $U > 0$ . The RPA spin susceptibility is

$$\chi_s(\omega, \vec{q}) = \frac{\chi_s^0(\omega, \vec{q})}{1 - U\chi_s^0(\omega, \vec{q})}. \quad (1)$$

where  $\chi_s^0(\omega, \vec{q})$  is the bare particle-hole bubble

$$\chi_s^0(\omega, \vec{q}) = - \int \frac{d^D k}{(2\pi)^D} \frac{n_F(\epsilon(\vec{k} + \vec{q})) - n_F(\epsilon(\vec{k}))}{i\omega + \epsilon(\vec{k} + \vec{q}) - \epsilon(\vec{k})} \quad (2)$$

with  $n_F$  the Fermi distribution. Sending  $\omega \rightarrow 0$  and afterwards  $\vec{q} \rightarrow 0$ , we get

$$\chi_s^0(\omega = 0, \vec{q} \rightarrow 0) = - \int \frac{d^D k}{(2\pi)^D} \frac{d}{d\epsilon} n_F(\epsilon(\vec{k})) = \int dE \rho(E) \delta_T(E) \quad (3)$$

where  $\delta_T(E) = -\frac{d}{dE} n_F(E) = (4T \cosh^2(E/2T))^{-1}$  becomes the delta function as  $T \rightarrow 0$ . If the density of states  $\rho$  is continuous, we get, at  $T = 0$ ,  $\chi_s(\omega = 0, \vec{q} \rightarrow 0) = \rho(0)/(1 - \rho(0)U)$ . The pole in this expression leads to the simple Stoner criterion

$$U\rho(0) \geq 1 \quad (4)$$

for a ferromagnetic ground state.

Of course, it is well known that the Stoner criterion overestimates the tendency towards ferromagnetism, and one should include correlation effects. One of them is that in (4),  $U$  is expected to get replaced by an effective Stoner coupling  $U_{\text{Stoner}}$ . This was first discussed in the so-called  $T$ -matrix approximation by Kanamori<sup>30</sup>. On the other hand, the  $T$ -matrix approximation also sums only a subclass of diagrams of one-loop type. Thus the natural question arises whether by RG methods one could perform a consistent resummation of all one-loop contributions, to treat the ferromagnetic tendencies and the screening together with other possibly competing tendencies.

Let us attempt to apply a one-loop momentum-shell scheme to the Stoner problem. The divergence of the uniform spin susceptibility is equivalent to a pole in the RPA perturbation series for the forward scattering amplitude  $a^a(\vec{k}, \vec{k}', \vec{q} \rightarrow 0)$  which is obtained from the antisymmetric irreducible two-particle scattering vertex  $\Gamma^{(4)}$  via

$$\begin{aligned} a^a(\vec{k}, \vec{k}') &= \lim_{\vec{q} \rightarrow 0} \Gamma^{(4)} \left[ (\vec{k} + \vec{q}, s, \vec{k}', -s) \rightarrow (\vec{k}, -s, \vec{k}' + \vec{q}, s) \right] \\ &= \lim_{\vec{q} \rightarrow 0} \left\{ \Gamma^{(4)} \left[ (\vec{k} + \vec{q}, s, \vec{k}', s) \rightarrow (\vec{k}, s, \vec{k}' + \vec{q}, s) \right] - \Gamma^{(4)} \left[ (\vec{k} + \vec{q}, s, \vec{k}', -s) \rightarrow (\vec{k}, s, \vec{k}' + \vec{q}, -s) \right] \right\}. \end{aligned} \quad (5)$$

Since the  $\vec{q} \rightarrow 0$  particle-hole loop is the only diagram occurring in the RPA calculation of  $a^a(\vec{k}, \vec{k}')$  and also in the RPA calculation leading to the Stoner criterion, we can limit the RG analysis to this channel, in complete analogy to Cooper or SDW (spin density wave) instabilities, where the ladder summation of the zero-total-momentum particle-particle diagram or the particle-hole diagram with the appropriate momentum transfer, respectively, are written as

solutions of the one-loop RG equation for the corresponding channel only (as indicated above, we do a study taking into account all contributions below). The RG equation is then the differential equation

$$\frac{\partial}{\partial \Lambda} U_\Lambda = -R_\Lambda U_\Lambda^2, \quad (6)$$

where  $R_\Lambda(\omega, \vec{q})$  is given by the integral for  $\chi_s^0$ , but with the integrand containing an additional factor  $\frac{\partial}{\partial \Lambda}[h(\epsilon(\vec{k} + \vec{q})/\Lambda)h(\epsilon(\vec{k})/\Lambda)]$ , with  $h(x)$  the cutoff function, say,  $h(x) = 0$  for  $|x| \leq 1$ . In the limit of interest for FM,

$$R_\Lambda(\omega = 0, \vec{q} \rightarrow 0) = \frac{\partial}{\partial \Lambda} F_\Lambda(T), \quad F_\Lambda(T) = \int dE \rho(E) \delta_T(E) h(E/\Lambda)^2, \quad (7)$$

and (6) integrates to

$$U_\Lambda = \frac{U_{\Lambda_0}}{1 - U_{\Lambda_0}(F_\Lambda(T) - F_{\Lambda_0}(T))} \quad (8)$$

If  $\Lambda_0$  is larger than the bandwidth,  $F_{\Lambda_0}(T) = 0$ . For  $\Lambda \rightarrow 0$ ,  $F_\Lambda(T) \rightarrow \chi_s^0(0, 0)$ , given by (3), so we recover exactly the RPA result, and thus the Stoner criterion.

However, a closer look at (7) reveals that  $F_\Lambda(T)$  is negligibly small for all scales  $\Lambda$  above  $O(T)$  because  $\delta_T(E) \leq e^{-|E|/T}$  and the cutoff function  $h$  restricts to  $|E| \geq \Lambda$ . Thus the contribution to the RPA is built up only at the very lowest scales of the flow: small- $\vec{q}$  particle-hole fluctuations, such as ferromagnetic tendencies, occur only at low RG scales  $\Lambda \approx T^{31,33}$ . For the derivation of the RPA as a solution to an approximate RG, this is not a problem. But our goal is to understand the interplay of different instabilities, and it can happen that another instability driven by terms that contribute to the flow at higher scales gives rise to a flow to strong coupling at scales  $\Lambda > T$ . Then the small- $\vec{q}$  contributions would remain unintegrated because, as discussed above, we have to stop the one-loop scheme once the couplings cease to be small. This appears to be particularly unjustified if the density of states (DOS) at the FS is much larger than the DOS at higher band energies, e.g. in cases where the FS is close to a van Hove singularity.

One can argue that this problem is not only due to the one-loop approximation but that it also has to do with restricting to  $\vec{q} = 0$ . If  $|\vec{q}|$  is of order  $\Lambda/v_F$ , the infrared cutoff does not suppress the particle-hole susceptibility any more. Thus one problem is the nonuniformity in the buildup of the function of  $\vec{q}$ , and one might think that averaging over  $\vec{q}$  in a region of size  $O(\Lambda/v_F)$  may help.

However, in this paper we attack the problem directly: as we shall show, in the temperature-flow RG scheme, the small  $\vec{q}$  fluctuations are properly taken into account directly, without further approximations like the averaging mentioned above.

In the next section, we set up the exact RG equation for the temperature-flow, and describe the one-loop approximation. After considering simple examples we apply the scheme to the two-dimensional  $t$ - $t'$  repulsive Hubbard model on the square lattice. This model is interesting because it supports a variety of fluctuations which can become singular at low temperatures and an unbiased treatment is highly desirable. On one hand it shows strong antiferromagnetic fluctuations due to partial nesting of the Fermi surface at finite wavevectors and omnipresent superconducting instabilities at low temperatures are enhanced by the anisotropic scattering. On the other hand the 2D Hubbard model is also a good candidate for a ferromagnetic ground state even at weak coupling because of the large density of states at the Fermi surface for certain particle densities.

## II. FORMALISM

Here we derive differential equations which determine the evolution of the 1PI (one-particle-irreducible) vertex functions with varying temperature. A perturbative RG scheme describing the change of the 1PI functions with variation of a general parameter-dependent quadratic part of the free action,  $S_0^{(2)}$ , was described in Refs. 34 and 15. In these applications the continuous change in  $S_0^{(2)}$  corresponded to integrating out modes with band energy at the running RG scale  $\Lambda$ . Here we show how the same RG equations can be used to describe the variation of the 1PI vertex functions with changing temperature. In this case the scale parameter can be directly taken as the temperature of the model system.

Consider a fermionic system on a 2D lattice at temperature  $T$ , with action

$$S = T \sum_n \sum_s \int \frac{d^2 k}{(2\pi)^2} \bar{\psi}_s(\vec{k}, i\omega_n) (i\omega_n - \epsilon_{\vec{k}}) \psi_s(\vec{k}, i\omega_n)$$

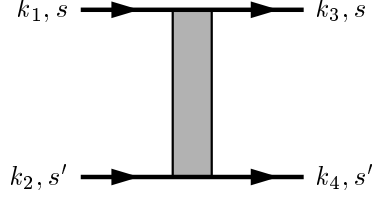


FIG. 1. The coupling function  $V(\vec{k}_1, \vec{k}_2, \vec{k}_3)$ .  $\vec{k}_4$  is fixed by wavevector conservation on the lattice.

$$\begin{aligned}
& + \frac{1}{2} T^3 \sum_{n_1, n_2, n_3} \sum_{s, s'} \int \frac{d^2 k_1}{(2\pi)^2} \frac{d^2 k_2}{(2\pi)^2} \frac{d^2 k_3}{(2\pi)^2} V(\vec{k}_1, \vec{k}_2, \vec{k}_3) \bar{\psi}_s(\vec{k}_3, i\omega_{n_3}) \bar{\psi}_{s'}(\vec{k}_4, i\omega_{n_4}) \psi_{s'}(\vec{k}_2, i\omega_{n_2}) \psi_s(\vec{k}_1, i\omega_{n_1}) \\
& + \sum_n \sum_s \int \frac{d^2 k}{(2\pi)^2} \left[ \bar{\psi}_s(\vec{k}, i\omega_n) \xi_s(\vec{k}, i\omega_n) + \psi_s(\vec{k}, i\omega_n) \bar{\xi}_s(\vec{k}, i\omega_n) \right]. \tag{9}
\end{aligned}$$

Here  $\bar{\psi}$  and  $\psi$  are anticommuting Grassmann fields and the Matsubara frequencies  $\omega_n = (2n + 1)\pi T$  are summed over all integer  $n$ . We have assumed spin-rotation-invariant and frequency-independent interactions. Further we have added source fields  $\bar{\xi}$  and  $\xi$ . Obviously both the quadratic and the quartic part of the action depend on the temperature  $T$ .

We now recall the case where only the quadratic part of the action depends on an additional continuous parameter  $\Lambda$ . Formally we go from  $S$  to a  $\Lambda$ -dependent action  $S_\Lambda$  by replacing

$$T \left[ i\omega - \epsilon(\vec{k}) \right] \longrightarrow Q_\Lambda(i\omega, \vec{k}). \tag{10}$$

One can then derive RG differential equations describing the variation of the 1PI vertex functions with  $\Lambda$ . These equations are obtained from the  $\Lambda$ -dependent Legendre transform

$$\Gamma_\Lambda(\phi, \bar{\phi}) = W_\Lambda(\xi, \bar{\xi}) - \sum_n \sum_s \int \frac{d^2 k}{(2\pi)^2} \left[ \bar{\phi}_s(\vec{k}, i\omega_n) \xi_s(\vec{k}, i\omega_n) + \phi_s(\vec{k}, i\omega_n) \bar{\xi}_s(\vec{k}, i\omega_n) \right], \tag{11}$$

of the generating functional of the connected non-amputated  $m$ -point Green functions  $W^{(m)}$ ,

$$e^{-W_\Lambda(\xi, \bar{\xi})} = \int D\psi D\bar{\psi} e^{-S_\Lambda(\psi, \bar{\psi}, \xi, \bar{\xi})}. \tag{12}$$

Here we abbreviate the notation and define a combined index  $p = (i\omega_n, \vec{k}, s)$ , moreover  $\int dp = \sum_{n,s} \int \frac{d^2 k}{(2\pi)^2}$ . The RG differential equations describing the evolution of the selfenergy  $\Sigma_\Lambda(p)$  and coupling function  $V_\Lambda(p_1, p_2, p_3)$  with  $p_4 = p_1 + p_2 - p_3$  (from which the fully antisymmetric four-point vertex can be reconstructed<sup>34</sup>, see also Fig. 1) with variation of that parameter read

$$\frac{d}{d\Lambda} \Sigma_\Lambda(p) = \int dp' S_\Lambda(p') [V_\Lambda(p, p', p') - 2V_\Lambda(p, p', p)] \tag{13}$$

and

$$\frac{d}{d\Lambda} V_\Lambda(p_1, p_2, p_3) = \mathcal{T}_{PP,\Lambda} + \mathcal{T}_{PH,\Lambda}^d + \mathcal{T}_{PH,\Lambda}^{cr} \tag{14}$$

with

$$\begin{aligned}
& \mathcal{T}_{PP,\Lambda}(p_1, p_2; p_3, p_4) = \\
& - \int dp V_\Lambda(p_1, p_2, p) L(p, -p + p_1 + p_2) V_\Lambda(p, -p + p_1 + p_2, p_3) \tag{15}
\end{aligned}$$

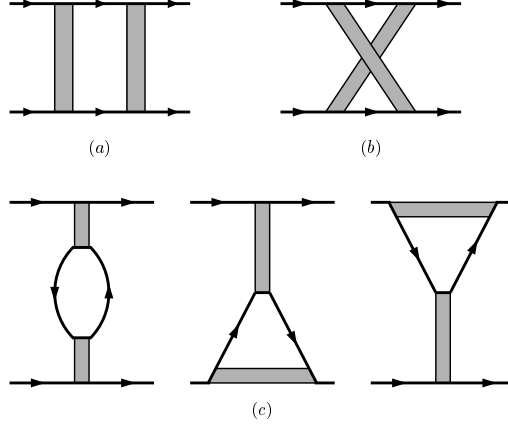


FIG. 2. The particle-particle and particle-hole diagrams contributing to the one-loop RG equation.

$$\begin{aligned}
& \mathcal{T}_{PH,\Lambda}^d(p_1, p_2; p_3, p_4) = \\
& - \int dp \left[ -2V_\Lambda(p_1, p, p_3) L(p, p + p_1 - p_3) V_\Lambda(p + p_1 - p_3, p_2, p) \right. \\
& \quad + V_\Lambda(p_1, p, p + p_1 - p_3) L(p, p + p_1 - p_3) V_\Lambda(p + p_1 - p_3, p_2, p) \\
& \quad \left. + V_\Lambda(p_1, p, p_3) L(p, p + p_1 - p_3) V_\Lambda(p_2, p + p_1 - p_3, p) \right] \quad (16)
\end{aligned}$$

$$\begin{aligned}
& \mathcal{T}_{PH,\Lambda}^{cr}(p_1, p_2; p_3, p_4) = \\
& - \int dp V_\Lambda(p_1, p + p_2 - p_3, p) L(p, p + p_2 - p_3) V_\Lambda(p, p_2, p_3) \quad (17)
\end{aligned}$$

In these equations,

$$L(p, p') = S_\Lambda(p) W_\Lambda^{(2)}(p') + W_\Lambda^{(2)}(p) S_\Lambda(p') \quad (18)$$

with the so-called single-scale propagator

$$S_\Lambda(p) = -W_\Lambda^{(2)}(p) \left[ \frac{d}{d\Lambda} Q_\Lambda(p) \right] W_s^{(2)}(p). \quad (19)$$

The one-loop diagrams corresponding to the terms (15), (16) and (17) are shown in Fig. 2.

In the typical momentum-shell RG, the varying parameter  $\Lambda$  is an energy scale which separates high and low energy modes. The strategy is to integrate out the high energy modes first. In this case the scale parameter only affects the quadratic part  $Q_\Lambda(p)$ , which is multiplied with an appropriate cutoff function. Here, for the reasons discussed in the introduction, we want to treat the temperature as varying parameter. Our reasoning is as follows: at high temperatures, where  $\pi T$  is larger than the bandwidth and the interaction energies, perturbation theory converges, and moreover the corrections to the selfenergy and four-point function are of order  $1/T$ , hence small. Thus at high temperature, the vertex functions are essentially identical to the terms in the action. Then we track the renormalization of the vertex functions when the temperature is lowered. Of course this idea is implicit in most of the well-known scaling approaches<sup>4</sup>. On a technical level however this strategy has usually been cast into some cutoff-variation procedure with similar results as the more elaborate modern Wilsonian schemes.

In order to apply the RG scheme for the 1PI vertex functions with  $T$  as a flow parameter we first have to perform a transformation which shifts all temperature dependence to the quadratic part of the action.

### A. New fields

The  $T^3$ -factor in the interaction part can be removed by transforming the action to the new fermionic fields given by

$$\bar{\eta}_s(\vec{k}, n) = T^{3/4} \bar{\psi}_s(\vec{k}, i\omega_n), \quad \eta_s(\vec{k}, n) = T^{3/4} \psi_s(\vec{k}, i\omega_n). \quad (20)$$

The source fields are chosen to transform according to

$$\bar{\zeta}_s(\vec{k}, n) = T^{-3/4} \bar{\xi}_s(\vec{k}, i\omega_n), \quad \zeta_s(\vec{k}, n) = T^{-3/4} \xi_s(\vec{k}, i\omega_n). \quad (21)$$

The action then reads

$$\begin{aligned} S = & T^{-1/2} \sum_n \sum_s \int \frac{d^2 k}{(2\pi)^2} \bar{\eta}_s(\vec{k}, n) (i\omega_n - \epsilon_{\vec{k}}) \eta(\vec{k}, n) \\ & + \frac{1}{2} \sum_{n_1, n_2, n_3} \sum_{s, s'} \int \frac{d^2 k_1}{(2\pi)^2} \frac{d^2 k_2}{(2\pi)^2} \frac{d^2 k_3}{(2\pi)^2} V(\vec{k}_1, \vec{k}_2, \vec{k}_3) \bar{\eta}_s(\vec{k}_3, n_3) \bar{\eta}_{s'}(\vec{k}_4, n_4) \eta_{s'}(\vec{k}_2, n_2) \eta_s(\vec{k}_1, n_1) \\ & + \sum_n \sum_s \int \frac{d^2 k}{(2\pi)^2} \left[ \bar{\eta}_s(\vec{k}, n) \zeta_s(\vec{k}, n) + \eta_s(\vec{k}, n) \bar{\zeta}_s(\vec{k}, n) \right]. \end{aligned} \quad (22)$$

Only the quadratic part depends on the temperature. The connected  $m$ -point correlation functions  $W_\psi^{(m)}$  and  $W_\eta^{(m)}$  are related as follows (the change in the integration measure drops out):

$$\begin{aligned} W_\psi^{(m)}(\vec{k}_1, i\omega_{n_1}, \dots, \vec{k}_m, i\omega_{n_m}) &= \langle \psi_{s_1}(\vec{k}_1, i\omega_{n_1}) \dots \bar{\psi}_{s_m}(\vec{k}_m, i\omega_{n_m}) \rangle \\ &= T^{-3m/4} \langle \eta_{s_1}(\vec{k}_1, n_1) \dots \bar{\eta}_{s_m}(\vec{k}_m, n_m) \rangle \\ &= T^{-3m/4} W_\eta^{(m)}(\vec{k}_1, n_1, \dots, \vec{k}_m, n_m). \end{aligned} \quad (23)$$

Using the action in terms of the new fields we can now apply the RG formalism from Ref. 34. This yields the flow of vertex functions  $\Gamma_\eta^{(m)}(\vec{k}_1, n_1, \dots, \vec{k}_m, n_m)$  when we change the temperature. Since they are the expansion coefficients of  $\Gamma_s$ , which is a functional of fields conjugated to the  $\zeta$  source fields, the  $\Gamma_\eta^{(m)}$  are related to the vertex functions of the  $\psi$  fields via

$$\Gamma_\psi^{(m)}(\vec{k}_1, i\omega_{n_1}, \dots, \vec{k}_m, i\omega_{n_m}) = T^{3m/4} \Gamma_\eta^{(m)}(\vec{k}_1, n_1, \dots, \vec{k}_m, n_m), \quad (24)$$

in particular

$$\Gamma_\psi^{(2)}(\vec{k}_1, i\omega_{n_1}, \vec{k}_2, i\omega_{n_2}) = T^{3/2} \Gamma_\eta^{(2)}(\vec{k}_1, n_1, \vec{k}_2, n_2) \quad (25)$$

and

$$\Gamma_\psi^{(4)}(\vec{k}_1, i\omega_{n_1}, \dots, \vec{k}_4, i\omega_{n_4}) = T^3 \Gamma_\eta^{(4)}(\vec{k}_1, n_1, \dots, \vec{k}_4, n_4). \quad (26)$$

Let us consider an example. If the interaction term at temperature  $T$  is taken to be

$$\frac{1}{2} T^3 \sum_{n_1, n_2, n_3} \sum_{s, s'} \int \frac{d^2 k_1}{(2\pi)^2} \frac{d^2 k_2}{(2\pi)^2} \frac{d^2 k_3}{(2\pi)^2} V_T(\vec{k}_1, \vec{k}_2, \vec{k}_3) \bar{\psi}_s(\vec{k}_3, i\omega_{n_3}) \bar{\psi}_{s'}(\vec{k}_4, i\omega_{n_4}) \psi_{s'}(\vec{k}_2, i\omega_{n_2}) \psi_s(\vec{k}_1, i\omega_{n_1}), \quad (27)$$

the antisymmetric four-point vertex in the  $\psi$ -fields reads<sup>34</sup>, to first order in the interaction,

$$\Gamma_{\psi, T}^{(4)}(\vec{k}_1, s, i\omega_{n_1}; \vec{k}_2, s', i\omega_{n_2}; \vec{k}_3, s, i\omega_{n_3}; \vec{k}_4, s', i\omega_{n_4}) = T^3 \left[ V_T(\vec{k}_1, \vec{k}_2, \vec{k}_3) - \delta_{s, s'} V_T(\vec{k}_2, \vec{k}_1, \vec{k}_3) \right]. \quad (28)$$

The four-point vertex for the  $\eta$ -fields is simply

$$\Gamma_{\eta, T}^{(4)}(\vec{k}_1, s, n_1; \vec{k}_2, s', n_2; \vec{k}_3, s, n_3; \vec{k}_4, s', n_4) = T^{-3} \Gamma_{\psi, T}^{(4)}(\vec{k}_1, s, i\omega_{n_1}; \vec{k}_2, s', i\omega_{n_2}; \vec{k}_3, s, i\omega_{n_3}; \vec{k}_4, s', i\omega_{n_4}), \quad (29)$$

hence of order  $T^0$ , and it contains the coupling function  $V_T$ . Thus the RG equations for the four-point-vertex in terms of the  $\eta$ -fields exactly yield the flow of the coupling function, and we can use the relations (24) to express the results in terms of the original vertex functions.

In this paper, like in Refs. 15 and 16, we will neglect selfenergy corrections to the flow and furthermore truncate the infinite hierarchy of RG equations for the  $m$ -point vertex functions by setting all 1PI vertex function higher than fourth order equal to zero. These approximations restrict the validity of the results to the weakly coupled and weakly correlated regime. We also drop the frequency dependence of the four-point vertex.

## B. The single-scale propagator

The quadratic part of the action expressed in the  $\eta$ -fields reads  $Q_{\eta,T}(\vec{k}, n) = T^{-1/2}(i\omega_n - \epsilon_{\vec{k}})$ . In absence of selfenergy corrections, we obtain

$$W_{\eta,T}^{(2)}(\vec{k}, n) = \frac{T^{1/2}}{i\omega_n - \epsilon_{\vec{k}}}. \quad (30)$$

Therefore the single-scale propagator is given by

$$S_T(\vec{k}, n) = -W_{\eta,T}^{(2)}(\vec{k}, n) \left[ \frac{d}{dT} Q_{\eta,T}(\vec{k}, n) \right] W_{\eta,T}^{(2)}(\vec{k}, n) = -\frac{T^{-1/2}}{2} \frac{i\omega_n + \epsilon(\vec{k})}{[i\omega_n - \epsilon(\vec{k})]^2}. \quad (31)$$

## C. One-loop diagrams

Next, consider the product of two fermion propagators  $L(p, p')$  defined in (18), which appears in the RG equation described in 34. The index  $p$  contains the frequency  $\omega$  and wavevector  $\vec{k}$ , at band energy  $\epsilon$  associated to one propagator and  $p'$  the frequency  $\omega'$ , wavevector  $\vec{k}'$  at band energy  $\epsilon'$  associated to the other one. Inserting (30) and (31) into (18), we have

$$L(p, p') = -\frac{1}{2} \left[ \frac{i\omega + \epsilon}{(i\omega - \epsilon)^2} \frac{1}{i\omega' - \epsilon'} + \frac{1}{i\omega - \epsilon} \frac{i\omega' + \epsilon'}{(i\omega' - \epsilon')^2} \right] = \frac{\omega\omega' + \epsilon\epsilon'}{(i\omega - \epsilon)^2(i\omega' - \epsilon')^2} = \frac{d}{dT} \left[ T \frac{1}{i\omega - \epsilon} \frac{1}{i\omega' - \epsilon'} \right]. \quad (32)$$

The terms on the right hand side of the flow equation are of the form

$$\int dp L(p, p') \Phi(\vec{k}, s, \vec{k}', s') = \int \frac{d^2k}{(2\pi)^2} \sum_{s, s'} \frac{d}{dT} \left[ T \sum_n \frac{1}{i\omega_n - \epsilon(\vec{k})} \frac{1}{i\omega_{n'} - \epsilon(\vec{k}')} \right] \Phi(\vec{k}, s, \vec{k}', s'), \quad (33)$$

i.e. they are temperature derivatives of bubble diagrams. Thus, in order to calculate the temperature flow of the coupling function, we can think in terms of the usual one-loop diagrams of the perturbation expansion in the original  $\psi$ -fields and simply take the temperature derivative of the particle-hole and particle-particle bubbles.

## III. SIMPLE EXAMPLES

Here we apply the scheme to two simple examples and show that it yields the results expected from direct perturbation expansions. In particular we describe how the temperature-flow scheme allows us to describe Cooper and ferromagnetic instabilities in an analogous fashion.

### A. Cooper instability

Here we show that for a small attractive electron-electron interaction at temperature  $T_0$  the formalism leads to a Cooper instability at lower temperature  $T_c$ . We assume that at  $T = T_0$  the action is given by the BCS model,

$$S_{T_0} = T_0 \sum_n \int \frac{d^2k}{(2\pi)^2} \bar{\psi}(\vec{k}, i\omega_n) (i\omega_n - v_F(k - k_F)) \psi(\vec{k}, i\omega_n) + \frac{1}{2} V_{T_0}^{\text{Cooper}} T_0^3 \sum_{n_1, n_2, n_3} \int \frac{d^2k}{(2\pi)^2} \int \frac{d^2k'}{(2\pi)^2} \bar{\psi}_s(\vec{k}', i\omega_{n_3}) \bar{\psi}_{-s}(-\vec{k}', i\omega_{n_4}) \psi_{-s}(-\vec{k}, i\omega_{n_2}) \psi_s(\vec{k}, i\omega_{n_1}). \quad (34)$$

Here,  $V_{T_0}^{\text{Cooper}} < 0$  is the attractive interaction between electrons with opposite wavevectors and the bandwidth  $W$  is taken such that  $v_F k_F - W > 0$ . We assume a linear dispersion. We are interested in the low-temperature behavior of the four-point vertex with zero incoming total momentum and frequency,

$$\Gamma_{\psi,T}^{(4)} \left[ (\vec{k}, s, -\vec{k}, -s) \rightarrow (\vec{k}', s, -\vec{k}', -s) \right] = T^3 V_T(\vec{k}, -\vec{k}, \vec{k}').$$

Focusing on the pairing channel, we neglect all particle-hole contributions. Therefore we are left with the temperature derivative of the particle-particle bubble and  $V_T(\vec{k}, -\vec{k}, \vec{k}') = V_T^{\text{Cooper}}$  remains independent of  $\vec{k}$  and  $\vec{k}'$ . The RG equation for  $V_T^{\text{Cooper}}$  involves the particle-particle bubble  $\Pi(\omega, \vec{q})$  with  $\omega = 0$  and pair momentum  $\vec{q} = 0$ . Using the results from Sec. II C it reads

$$\frac{d}{dT} V_T^{\text{Cooper}} = -V_T^{\text{Cooper}} \frac{d}{dT} \Pi(0, 0) = -V_T^{\text{Cooper}} \frac{d}{dT} \int_{-W}^W d\epsilon \rho(\epsilon) \frac{1 - 2n_F(\epsilon)}{2\epsilon}. \quad (35)$$

We can immediately integrate it, similarly to (7), to get

$$-\frac{1}{V_T^{\text{Cooper}}} \Big|_{T_0}^T = - \int_{-W}^W d\epsilon \rho(\epsilon) \frac{1 - 2n_F(\epsilon)}{2\epsilon} \Big|_{T_0}^T. \quad (36)$$

Assuming that the bandwidth  $W$  is much larger than the temperature and that the density of states is a constant  $\rho_0$ , the integral is logarithmic and

$$V_T^{\text{Cooper}} = \frac{V_{T_0}^{\text{Cooper}}}{1 - \rho_0 V_{T_0}^{\text{Cooper}} \log(T/T_0)}. \quad (37)$$

Thus, starting with an attractive interaction  $V_{T_0}^{\text{Cooper}} < 0$  at a higher temperature  $T_0 \ll W$  we obtain a pole in the effective  $s$ -wave Cooper pair scattering at

$$T_c = T_0 \exp \left[ -\frac{1}{\rho_0 |V_{T_0}^{\text{Cooper}}|} \right]. \quad (38)$$

This result is analogous to the ladder summation from straightforward perturbation theory when we replace  $T_0$  with the Debye frequency and identify the initial interaction  $V_{T_0}^{\text{Cooper}}$  at this temperature with the bare attractive electron-electron interaction  $V_0^{\text{Cooper}}$ , e.g. mediated through phonon-exchange. Although these identifications cannot be justified directly within a microscopic model with a specific Hamiltonian, they appear to be highly plausible for an effective description of the system.

In fact one can obtain the BCS relation

$$T_c = 1.14W \exp \left[ -\frac{1}{\rho_0 |V_{T_0}^{\text{Cooper}}|} \right] \quad (39)$$

as well if one assumes that  $T_0 \gg W$ . In that case, inserting  $T_0$  in the right hand side of (36) gives zero because at high temperatures  $n_F \approx 1/2$ . Thus we recover the linearized BCS gap equation<sup>35</sup> at  $T_c$ ,

$$\frac{1}{\rho_0 |V_{T_0}^{\text{Cooper}}|} = \int_{-W}^W d\epsilon \frac{1 - 2n_F(\epsilon)}{2\epsilon}, \quad (40)$$

as a condition for a divergence of  $V_T^{\text{Cooper}}$  at  $T = T_c$ . From solving (40), one obtains (39).

## B. Stoner instability

Next we consider the instability towards ferromagnetism in a Hubbard-type system with repulsive onsite interaction  $U_{\text{eff}}$ . We show that for a logarithmically divergent density of states within an effective bandwidth  $W_{\text{eff}}$ ,

$$\rho(\epsilon) = \bar{\rho} \log \frac{W_{\text{eff}}}{|\epsilon|}, \quad (41)$$

an approximation to the RG equation reproduces the Stoner instability obtained by straightforward perturbation theory. In the latter treatment one sums up the particle-hole bubbles for momentum transfer  $\vec{q} \rightarrow 0$  with the

intermediate particles having band energies within  $\pm W_{\text{eff}}$ . The van Hove singularity in the density of states causes a breakdown of the paramagnetic state at temperatures below

$$T_c \sim W_{\text{eff}} \exp \left[ -\frac{1}{U_{\text{eff}} \bar{\rho}} \right]. \quad (42)$$

Analogous to the diagram summation we restrict the RG analysis to the crossed particle-hole channel with small momentum transfer. The Stoner instability should then appear as a divergence of the forward scattering amplitude  $a^a(\vec{k}, \vec{k}', \vec{q} \rightarrow 0)$ , which is in our RG language given by

$$\lim_{\vec{q} \rightarrow 0} \Gamma_{\psi, T}^{(4)} \left[ (\vec{k}, s, \vec{k}' + \vec{q}, -s) \rightarrow (\vec{k}', s, \vec{k} + \vec{q}, -s) \right] = \lim_{\vec{q} \rightarrow 0} T^3 V_T(\vec{k}, \vec{k}' + \vec{q}, \vec{k}').$$

Next we will assume an isotropic system and write

$$\lim_{\vec{q} \rightarrow 0} V_T(\vec{k}, \vec{k}' + \vec{q}, \vec{k}') = V_T^{\text{FM}}.$$

Using Eq. (3) with (41), the RG equation for this coupling function reads

$$\frac{d}{dT} V_T^{\text{FM}} = -V_T^{\text{FM}}{}^2 \frac{d}{dT} \chi_s(0, \vec{q} \rightarrow 0) = -V_T^{\text{FM}}{}^2 \frac{d}{dT} \int_{-W}^W d\epsilon \rho(\epsilon) \frac{d}{d\epsilon} n_F(\epsilon). \quad (43)$$

Note the similarity of, but also the difference between, (43) and (7) – both equations have the same form, but there is no cutoff function in (43). Integration of (43) gives

$$\frac{1}{V_{T_0}^{\text{FM}}} - \frac{1}{V_T^{\text{FM}}} = F(T) - F(T_0), \quad (44)$$

with

$$F(T) = \chi_s^0(0, 0) = \int dE \rho(E) \delta_T(E) \quad (45)$$

Because  $\delta_T(E) \propto T^{-1}$ ,  $F(T_0)$  vanishes as  $T_0 \rightarrow \infty$ , hence we recover for large  $T_0$  the RPA result

$$V_T^{\text{FM}} = \frac{V_{T_0}^{\text{FM}}}{1 - V_{T_0}^{\text{FM}} F(T)} \quad (46)$$

In the case of the density of states (41), we can also use integration by parts to get, for  $T_0 \ll W$ ,

$$\frac{d}{dT} V_T^{\text{FM}} = -V_T^{\text{FM}}{}^2 \bar{\rho} \int_{-W}^W d\epsilon \frac{1}{\epsilon} \frac{d}{dT} n_F(\epsilon) = V_T^{\text{FM}}{}^2 \bar{\rho} \frac{1}{T} \int_{-W}^W d\epsilon \frac{d}{d\epsilon} n_F(\epsilon).$$

The resulting differential equation is solved by

$$V_T^{\text{FM}} = \frac{V_{T_0}^{\text{FM}}}{1 + V_{T_0}^{\text{FM}} \bar{\rho} \log(T/T_0)}. \quad (47)$$

Analogous to the Cooper instability studied above, the initial interaction  $V_{T_0}$  at higher temperature  $T_0 \ll W$ , in this case repulsive, leads to a pole at

$$T_c = T_0 \exp \left[ -\frac{1}{\bar{\rho} V_{T_0}^{\text{FM}}} \right], \quad (48)$$

signaling the instability of the paramagnetic state with respect to spontaneous polarization. Again this result is in close analogy with the RPA summation when we replace the initial temperature  $T_0$  with the effective bandwidth  $W_{\text{eff}}$ . Of course this approximation to the RG equation can also lead to pole for a non-divergent density of states if the initial interaction is sufficiently strong. In this case, upon integrating from  $T_0 \gg W$  down towards  $T = 0$ , we encounter a pole if the simple Stoner criterion (4) is fulfilled.

Thus, in our RG treatment, the simple Stoner criterion can be derived as a consequence of an approximation to the one-loop RG equation where only the crossed particle-hole terms are kept. As we shall see in the next section, the full one-loop flow is more complicated, and one can thereby see the limitations of the naive Stoner criterion, and instances where it becomes invalid because of superconducting and antiferromagnetic tendencies.

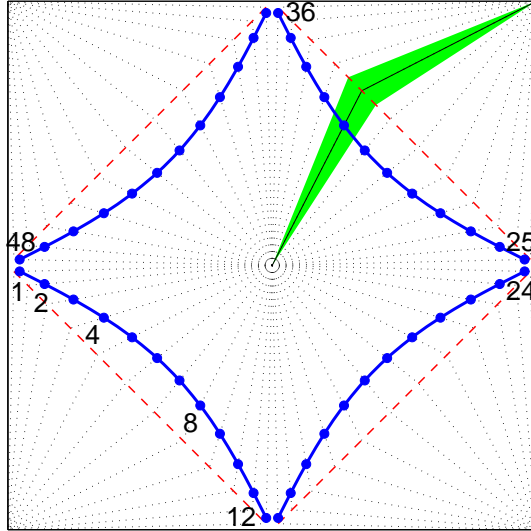


FIG. 3. The Brillouin zone, Fermi (solid line) and umklapp (dashed line) surface and the lines in the patch lines for  $N = 32$ . The circles denote the wave vectors for which the four-point vertex function is calculated. For all wave vectors inside the same patch (shaded region) around the lines,  $V_{\Lambda}(\vec{k}_1, \vec{k}_2, \vec{k}_3)$  is approximated by a constant.

#### IV. APPLICATION TO THE 2D HUBBARD MODEL

Here we apply the RG scheme to the 2D  $t$ - $t'$  Hubbard model. In our setup with the temperature as a flow parameter, this again means that we assume that at some higher temperature  $T_0$  the single-particle Green's function of the system is adequately described by

$$G_0(i\omega, \vec{k}) = \frac{1}{i\omega - \epsilon(\vec{k})}, \quad (49)$$

with the band dispersion  $\epsilon(\vec{k}) = -2t [\cos k_x + \cos k_y] - 4t' \cos k_x \cos k_y - \mu$  including nearest and next-nearest neighbor hoppings  $t$  and  $t'$ , respectively. The scattering vertex is given by a local repulsion

$$V_{T_0}(\vec{k}_1, \vec{k}_2, \vec{k}_3) = U. \quad (50)$$

Then by following the flow of the scattering vertex with lowering the temperature, we obtain information on the possible low-temperature phases of the system. In particular we analyze which classes of coupling functions and which susceptibilities become important at low temperatures. For a large parameter range, we observe a flow to strong coupling. This means that at sufficiently low temperatures some components of the coupling function  $V_T(\vec{k}_1, \vec{k}_2, \vec{k}_3)$  reach values larger than the bandwidth  $\approx 8t$ . The approximations made, i.e. the restriction to one-loop equations and the neglect of selfenergy corrections, fail when the couplings get too large. Therefore we stop the flow when the largest coupling exceeds a high value larger than the bandwidth, e.g.  $V_{T, \max} = 18t$ . This defines a *characteristic temperature*  $T_c$  of the flow to strong coupling. As it is well known, in two spatial dimensions breaking of continuous symmetries is impossible at  $T > 0$ . Thus the flow to strong coupling which we observe for a large part of the parameter range should either be interpreted as an indication of an ordered ground state of the corresponding type or as a tendency towards ordering at  $T \sim T_c$  for the case when an additional coupling term in the third spatial direction is included.

For the numerical integration of these coupled equations we apply a phase space discretization<sup>11,14-16</sup>. The 2D Brillouin zone (BZ) is divided up into  $N$  elongated patches centered around  $N$  lines. Each line connects the origin with one of the  $(\pm\pi, \pm\pi)$ -points with two straight pieces and a kink at the Umklapp surface (see Fig. 3).

Next we discretize the coupling function. We approximate  $V_T(\vec{k}_1, \vec{k}_2, \vec{k}_3)$  by a constant for all wave vectors in the same patches and calculate the RG flow for the subset of interaction vertices with one wavevector representative for each patch. We take these wave vectors as the crossing points of the  $N$  lines with the Fermi surface (FS). The phase space integrations are performed as sums over the patches and integrations over the radial direction along 3 or 5 lines inside each patch. Most calculations were using 48-patch systems. Calculations with 96 patches gave equivalent results. A typical Fermi surface with  $N = 48$  points is shown in Fig. 3.

The motivation for using this patch scheme is that the Fermion propagators are largest on the Fermi surface and decay away from it. Thus one can expect that by tracking the coupling functions for the wavevectors close to the Fermi surface the leading flow will be described accurately.

Together with the flow of the interactions we calculate several static susceptibilities by coupling external fields of appropriate form to the electrons. During the flow these external couplings are renormalized through one-loop vertex corrections, as described in Ref. 15. In this paper, we concentrate on the  $d_{x^2-y^2}$ - and  $p$ -wave pairing susceptibilities, the AF susceptibility  $\chi_s(\vec{q} = (\pi, \pi))$  and the FM susceptibility  $\chi_s(\vec{q} \rightarrow 0)$ .

## V. RESULTS FOR THE 2D HUBBARD MODEL AT THE VAN HOVE FILLING

Here we describe the results for the RG flow of the coupling function for the 2D Hubbard model with initial interaction  $U = 3t$  and varying value for the next-nearest neighbor hopping  $t'$ . The chemical potential  $\mu$  is fixed<sup>36</sup> at the van Hove value  $\mu = 4t'$  such the FS always contains the saddle points at  $(\pm\pi, 0)$  and  $(0, \pm\pi)$ . We start the RG scheme at temperature  $T_0 = 4t$  and integrate the coupled equations with decreasing temperature. We stop the flow when the largest coupling exceeds a high value larger than the bandwidth, e.g.  $V_{T, \text{max.}} = 18t$ , which defines the characteristic temperature for the flow to strong coupling,  $T_c$ .

The overall behavior of the flow to strong coupling is shown in Fig. 4. Focusing on AF,  $d$ -wave and FM susceptibilities, we observe three distinct parameter regions. The first, the AF regime, occurs closer to half band filling, for smaller absolute values of  $t' > -0.2t$ . Here the flow to strong coupling takes place at relatively high temperatures and the AF susceptibility is growing most strongly (see Fig. 5 for the Fermi surface and the flow of the susceptibilities). The dominant scattering processes at low  $T$  are given by AF processes between FS parts connected by wavevectors  $\approx (\pi, \pi)$ . These can be seen in the middle plot of Fig. 5 as bright features corresponding to strong repulsive couplings on the line  $\vec{k}_2 - \vec{k}_3 \approx (\pi, \pi)$ .

If we increase the absolute value of  $t'$  and adjust the chemical potential such that the FS remains at the van Hove points, the characteristic temperature  $T_c$  for the flow to strong coupling drops continuously and for  $t' < -0.2t$ , the  $d$ -wave susceptibility takes over as the leading susceptibility. In the flow of the couplings one clearly observes the dominant  $d_{x^2-y^2}$ -symmetry of the pair scattering, see the diagonal features in the middle plot of Fig. 6. For  $t' \approx -0.25t$  and a band filling slightly larger than the van Hove filling we again find a regime where the flow of  $d$ -wave and AF processes is strongly coupled similar as the saddle point regime studied in Ref. 15.

Here we focus on the flow at the van Hove filling when we increase the absolute value of  $t'$ . The characteristic temperature for the flow to strong coupling drops rapidly for  $t' \leq -0.3t$ , while for  $t' \geq -0.33t$  it rises again. For these values the flow to strong coupling is dominated by processes with small momentum transfer (middle plot in Fig. 7) and the FM susceptibility  $\chi_s(\vec{q} = 0)$  is by far the most divergent susceptibility at low temperatures (right plot in Fig. 7). The overall behavior strongly suggests a critical value for  $t'$  around  $t'_c \approx -0.33t$  where the ground state changes from  $d$ -wave singlet superconducting to ferromagnetic. We note that while our method allows, within the approximations made, to detect the instability of the Fermi liquid state against ferromagnetic fluctuations it does not give any information on the degree of the polarization of the ordered ground state.

Further we stress the fundamental difference of the qualitative change in the flow between the  $d$ -wave to the FM regime to the crossover from the AF to the  $d$ -wave regime: in the latter case the transition is continuous and takes place at relatively high scales. As emphasized in Refs. 15 and 16, for the FS close to the saddle points and away from half-filling, AF and  $d$ -wave tendencies do not compete but reinforce each other on the one-loop level, therefore one finds a gradual change in the character of the flow to strong coupling when  $t'$  is varied. There are strong indications<sup>15</sup> that the strong coupling state for a certain parameter range is not simply a symmetry-broken phase. In contrast with that, the transition from the  $d_{x^2-y^2}$ -wave regime to the FM regime at larger absolute values of  $t'$  is very distinct and - as suggested by our one-loop analysis - may be a quantum critical point of two mutually excluding tendencies. Due to the competition between singlet superconducting and ferromagnetic tendencies, the characteristic temperature for the flow to strong coupling becomes suppressed to smallest values around  $t'_c$ . The precise properties of the quantum critical point cannot be analyzed further for the time being because the numerical integration of the RG flow becomes rather time-consuming for these parameters.

The rivalry between singlet superconducting and FM tendencies is already foreshadowed on the  $d$ -wave side at  $t' \approx -0.3t$ . There the temperature-flow scheme yields much lower characteristic temperatures than the momentum-shell scheme used in Ref. 15 which is rather insensitive against the FM tendencies arising from the van Hove points for the reasons mentioned in the introduction.

The transition from singlet pairing to the ferromagnetic regime can also be seen in the flow of certain coupling functions which couple into both channels. For example let us take the component  $V_T(1, 25, 25)$  for a  $N = 48$  system (see Fig. 8). The incoming wavevectors  $\vec{k}_{F,1}$  and  $\vec{k}_{F,25}$  add up to zero, therefore the coupling corresponds to a Cooper

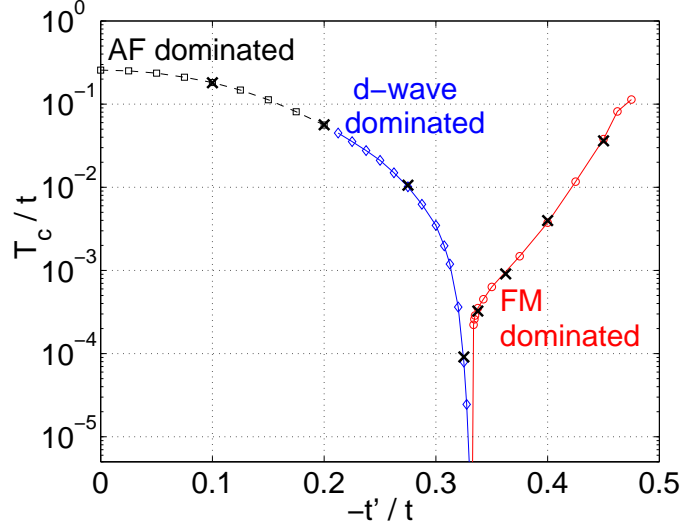


FIG. 4. Characteristic temperature  $T_c$  for the flow to strong coupling versus next nearest neighbor hopping amplitude  $t'$  from a 48-patch calculation (the crosses show data for 96 patches). The chemical potential is fixed at the van Hove value  $\mu = 4t'$ .  $T_c$  is defined as temperature where the couplings reach values larger than  $18t$ . For small  $|t'|$ , the instability is dominated by AF tendencies, for  $t' < -0.2t$  the  $d$ -wave tendencies prevail, and for  $t' < -0.33t$  the ferromagnetic fluctuations grow strongest. The criterion for the distinction between these regimes is taken as the derivative of the susceptibilities with respect to temperature at the scale where the couplings become larger than  $10t$ .

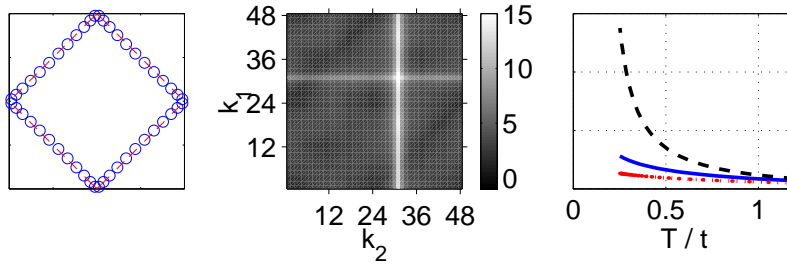


FIG. 5. Flow to strong coupling for  $t' = -0.025t$  and  $\mu = -0.1t$ . The left plot shows the 48 points on the Fermi surface (points 1, 12, 13, 24 etc. are closest to the saddle points). The middle plot shows the coupling function  $V_T(k_1, k_2, k_3)$  at low  $T$  as a function of the two incoming wavevectors labeled by  $k_1$  and  $k_2$  moving around the FS.  $k_3$  is fixed at point 6 in the Brillouin zone diagonal. The colorbar denotes the value of the coupling function in units of  $t$ . The right plot shows the flow of the AF susceptibility (dashed line),  $d$ -wave susceptibility (solid line) and FM susceptibility (dotted line) as a function of the temperature  $T$ .

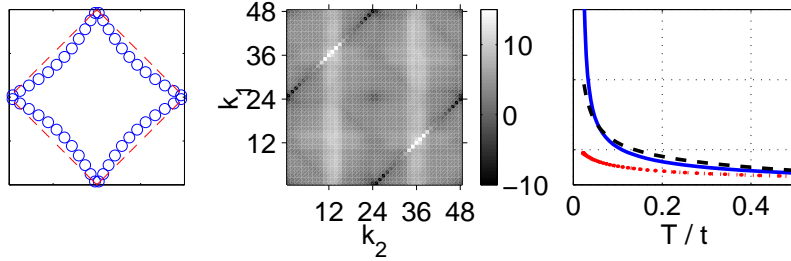


FIG. 6. Flow to strong coupling for  $t' = -0.25t$  and  $\mu = -t$ . The left plot shows the 48 points on the Fermi surface (points 1, 12, 13, 24 etc. are closest to the saddle points). The middle plot shows the coupling function  $V_T(k_1, k_2, k_3)$  at low  $T$  as a function of the two incoming wavevectors labeled by  $k_1$  and  $k_2$  moving around the FS.  $k_3$  is fixed at point 1 close to a saddle point. The colorbar denotes the value of the coupling function in units of  $t$ . The right plot shows the flow of the AF susceptibility (dashed line),  $d$ -wave susceptibility (solid line) and FM susceptibility (dotted line) as a function of the temperature  $T$ .

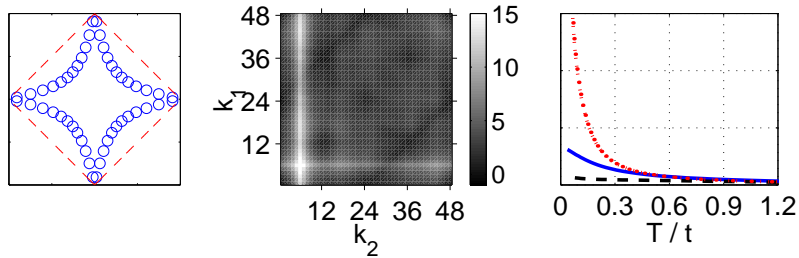


FIG. 7. Flow to strong coupling for  $t' = -0.45t$  and  $\mu = -1.8t$ . The left plot shows the 48 points on the Fermi surface (points 1, 12, 13, 24 etc. are closest to the saddle points). The middle plot shows the coupling function  $V_T(k_1, k_2, k_3)$  at low  $T$  as a function of the two incoming wavevectors labeled by  $k_1$  and  $k_2$  moving around the FS.  $k_3$  is fixed at point 6 in the Brillouin diagonal. The colorbar denotes the value of the coupling function in units of  $t$ . The right plot shows the flow of the AF susceptibility (dashed line),  $d$ -wave susceptibility (solid line) and FM susceptibility (dotted line) as a function of the temperature  $T$ .

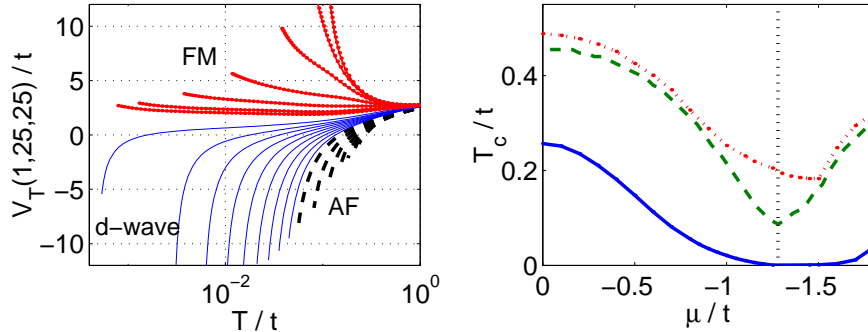


FIG. 8. Left: Flow of the forward scattering coupling function  $V_T(1, 25, 25)$  for the saddle point filling and different values of  $t'$ . The dashed (solid) lines correspond to the AF (d-wave) regime, where  $V_T(1, 25, 25)$  decreases when the temperature  $T$  is lowered, while the dotted lines correspond to the FM regime, where  $V_T(1, 25, 25)$  increases with decreasing  $T$ . Right: Characteristic temperature  $T_c$  for the flow to strong coupling versus  $t'$  at the van Hove filling  $\mu = 4t'$ . The lower curves (same as in Fig. 4) are obtained with the full one-loop RG, while the upper dotted line result from the RG where the particle-particle channel is left out. Right plot: Comparison of the flow of the FM susceptibility  $\chi_s(0)$  with and without particle-particle diagrams. For both cases, the RG equations were integrated until the couplings reach  $V_{T,\text{max.}} \approx 18t$ . The dashed line denotes the critical temperature from the generalized Stoner criterion. The vertical line at  $t' = -0.32t$  separates the FM regime from the AF in the Stoner calculation and RG without particle-particle diagrams.

process where a pair of electrons is scattered onto itself. Since wavevector  $\vec{k}_{F,1}$  is close to the saddle points it should rapidly diverge to  $-\infty$  if the flow is towards a  $d$ -wave superconducting ground state. On the other hand  $V_T(1, 25, 25)$  couples into the FM channel as well, as the momentum transfer between the second incoming and the first outgoing wavevector is the same (in the calculation we use a very small momentum transfer). In Landau-Fermi liquid language  $V_T(1, 25, 25)$  corresponds to the process  $a^a(\vec{k}_{F,1}, -\vec{k}_{F,1})$ , which should become large and positive if the flow signals a FM ground state. By plotting the flow of  $V_T(1, 25, 25)$  for the saddle point filling and different  $t'$ -values, as shown in Fig. 8 we can nicely observe the qualitative change in the flow when  $|t'|$  becomes larger than the critical value  $t'_c \approx -0.33t$ . We note that  $V_T(1, 25, 25)$  does not belong to the dominant scattering processes in the FM regime. The latter are given by forward scattering processes  $a^a(\vec{k}_F, \vec{k}'_F)$  with  $\vec{k}_F$  and  $\vec{k}'_F$  closer to the BZ diagonals (see Fig. 7) and grow more strongly towards  $T_c$ .

One can also investigate the contributions of different one-loop diagrams to the RG flow. Here we concentrate on the influence of the particle-particle channel on the flow. In the left plot of Fig. 8 we compare the characteristic temperatures for the full one-loop RG with the results when the particle-particle channel is left out. For all values of  $t'$ , the  $T_c$  is much higher, which shows clearly the importance of the particle-particle channel for a screening of the repulsive interaction. Without the particle-particle diagrams and close to  $t' = 0$  and  $t' = -0.5t$  the critical temperatures from the RG and from the generalized Stoner-criterion<sup>37</sup> are very similar. Again the FM susceptibility becomes dominant around  $t'_c \approx -0.33t$ , but without the particle-particle diagrams generating strong superconducting fluctuations, the characteristic temperature for the flow to strong coupling is only weakly suppressed for these parameters.

## VI. THE FLOW AWAY FROM THE VAN HOVE FILLING

Next we investigate the flow to strong coupling for band fillings away from the van Hove filling. The flow arising for smaller absolute values of the next-nearest neighbor hopping  $t'$  is very similar to the flow found with the momentum-shell techniques which has been extensively discussed in Refs.<sup>11,14-16</sup>. Therefore we now focus on the case  $t' < -0.33t$  where we find a flow dominated by ferromagnetic fluctuations at the van Hove filling. Changing the particle density moves the van Hove singularities away from the Fermi surface and one expects a reduction of the characteristic temperature for the flow to strong coupling accompanied with a decrease of the ferromagnetic tendencies. Furthermore, by similar arguments as for the interplay between antiferromagnetic and  $d$ -wave superconducting fluctuations when the FS nesting is reduced, one may presume that some kind of triplet superconducting channel might diverge at lower temperatures where the ferromagnetic tendencies get cut off. This expectation is confirmed by the results of the temperature-flow RG scheme.

The Cooper pair scattering  $V_T(\vec{k}, -\vec{k}, \vec{k}')$  transforms according to one of the 5 irreducible representations of the

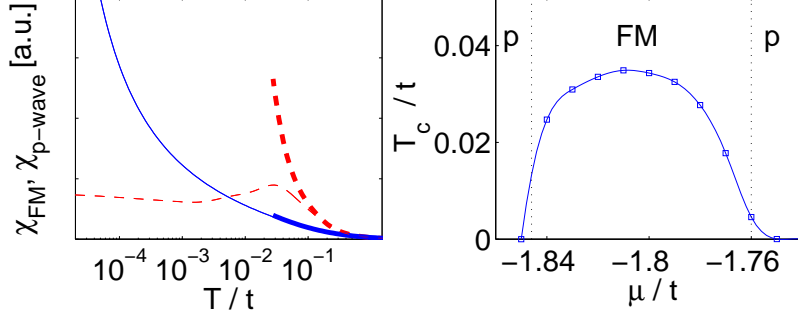


FIG. 9. Left plot: Flow of ferromagnetic (solid lines),  $p_x$ -wave (dashed lines) for  $t' = -0.45t$  at  $\mu = -1.78t$  (thick lines) and  $\mu = -1.74t$  (thin lines). Right plot: Critical temperature  $T_c$  where the largest couplings reach  $18t$  as function of the chemical potential  $\mu$ . The dotted vertical lines separate the parameter region where the FM or the  $p$ -wave susceptibility grow most strongly.

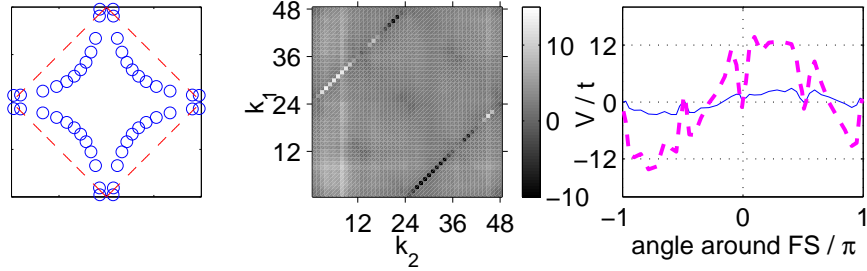


FIG. 10. Left panel: Fermi surface for  $\mu = -1.71t$  and  $t' = -0.45t$ . Middle panel: snapshot of the coupling function  $V(k_1, k_2, k_3)$  with  $k_3 = 6$  fixed in the Brillouin zone diagonal. Right panel: Pair scattering  $V(\vec{k}, -\vec{k}, \vec{k}_3)$  with  $\vec{k}$  varying around the Fermi surface at  $T = 1.1 \cdot 10^{-6}t$ . For the solid line  $\vec{k}_3$  is fixed at point 1 close to the saddle point  $(-\pi, 0)$  while for the dashed line,  $\vec{k}_3 \approx (-1.06, -0.86)$  is at point 6.

point group of the 2D square lattice. Among those there is the one-dimensional representation with  $d_{x^2-y^2}$ -symmetry important for smaller  $|t'|$  and the only two-dimensional representation transforming like  $p_x$  and  $p_y$ . In a solution of the BCS gap equation, components belonging to different representations do not mix, while e.g. within the  $p$ -representation components  $p_x \propto \cos\theta$  and  $p_y \propto \sin\theta$  and the higher harmonics  $\propto \cos 3\theta$  and  $\propto \sin 3\theta$  (also called  $f$ -wave) will occur together.

As the RG calculations down to low temperatures are rather time-consuming we limit ourselves to the exemplary case  $t' = -0.45t$  and leave a full investigation of the parameter space to future work. As shown in the right plot of Fig. 9 for  $t' = -0.45t$ , the critical temperature drops by several orders of magnitude when we increase the particle density per site from the VH value  $\langle n \rangle \approx 0.47$  at  $\mu = -1.8t$  to  $\langle n \rangle \approx 0.58$  at  $\mu = -1.7t$ . Further upon moving away from the VH filling, the growth of the FM susceptibility gets cut off and the  $p$ -wave triplet superconducting susceptibilities with symmetry  $p_x \propto \cos\theta$  or  $p_y \propto \sin\theta$  diverge at low temperature. Higher order harmonics  $\propto \cos 3\theta$  and  $\sin 3\theta$  diverge in a weaker fashion. The pair scattering at low temperatures in this parameter range is shown in Fig.10. One nicely observes that the pair scattering involving particles close to the saddle points is suppressed as the odd-parity nature of the  $p$ -wave pairing requires an opposite sign of the pair scattering  $V_T(\vec{k}, -\vec{k}, \vec{k}')$  e.g. for  $\vec{k}' \approx (0, \pi)$  and  $\vec{k} \approx (0, -\pi)$ . Comparing the temperature derivatives of ferromagnetic and superconducting susceptibilities when the leading couplings become larger than  $12t$ , the transition from the ferromagnetic to the  $p$ -wave superconducting regime occurs at a particle density of  $\langle n \rangle \approx 0.55$  per site. Again, very similar to the interplay between antiferromagnetic and  $d_{x^2-y^2}$  superconducting fluctuations for small  $|t'|$ , on the one-loop level there is a smooth evolution of the flow to strong coupling from the strongly FM dominated to the predominantly  $p$ -wave dominated instability. This suggests the presence of a transition between the two types of ordered states as a function of the band filling provided that symmetry-breaking at finite temperatures becomes possible in a three-dimensional environment. From our analysis the transition appears to be first order, but additional interaction effects beyond our one-loop calculation could change the behavior.

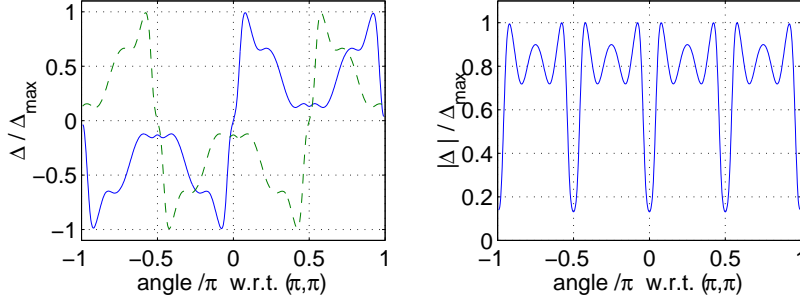


FIG. 11. Left panel: Angular variation of real (solid line) and imaginary (dashed line) part of the gap function obtained by the method explained in the text. Right panel: Angular variation of the gap magnitude. For these data,  $\mu = -1.71t$  and  $t' = -0.45t$ .

It is plausible to assume that the superconducting state for  $t' = -0.45t$  will be given by a nodeless superposition of the two components with symmetries  $p_x$  and  $p_y$ , which maximizes the condensation energy<sup>38</sup>. The direction of the Cooper pair spin or the  $\vec{d}(\vec{k})$ -vector parameterizing the odd-parity gap function remains indeterminate in the absence of spin-orbit coupling. Therefore six different pairing symmetries  $\vec{d}(\vec{k}) \propto \vec{x}k_x \pm \vec{y}k_y$ ,  $\propto \vec{x}k_y \pm \vec{y}k_x$  and  $\propto \vec{z}(k_x \pm ik_y)$  yield the same condensation energy and additional interactions like spin orbit coupling or the spin fluctuation feedback mechanism are needed to select one of these representations<sup>39</sup>. In any case the superconducting gap function for given  $s$  and  $s'$  will read

$$\Delta_{ss'}(\vec{k}) = \Delta_0(\vec{k}) (k_x \pm ik_y), \quad (51)$$

where the real prefactor  $\Delta_0(\vec{k})$  is unchanged under symmetry transformations of the lattice and takes care of the strong anisotropy within symmetry-related Fermi surface parts.

Our present method does not allow a straightforward calculation of the gap function in the superconducting state. Nevertheless we can use the Cooper pair scattering obtained from the RG flow as effective pair potential in a mean-field treatment of the superconducting state. Since the Cooper scattering diverges in our approach, this will not give any precise information on the overall magnitude of the energy gap, but it allows us to study the symmetry and the angular variation of the gap function. In Fig. 11 we show the solution of the BCS gap equation with symmetry given by Eq. (51) and using the rescaled Cooper pair scattering extracted from the RG in the case  $\mu = -1.71t$  and  $t' = -0.45t$ . For these data the angle is measured with respect to the  $(\pi, \pi)$ -point. Clearly the dips in the pair scattering at the saddle points mentioned above and observable in Fig. 10 lead to minima of the absolute gap magnitude on these FS parts. Thus the particular location of the FS close to the BZ boundary results in a highly anisotropic superconducting energy gap.

## VII. COMPARISON WITH OTHER APPROACHES AND CONCLUSIONS

We have described a modified RG scheme for interacting fermion systems which uses the temperature as explicit scaling parameter. In comparison with the momentum-shell schemes<sup>1,11,14,34</sup> the new approach has the advantage that it allows one to treat small- $\vec{q}$  singularities in the particle-hole channel, in our case corresponding to ferromagnetic tendencies, on the same basis as large- $\vec{q}$  (here antiferromagnetic) fluctuations or superconducting correlations.

At first sight the successive lowering of the temperature appears to be closer to the physical intuition than the reduction of an momentum-shell cutoff. On the other hand it should be mentioned that in general the initial conditions for the vertex function of the temperature-flow RG at the starting temperature do not exactly equal the vertex functions (to some order) of the microscopic Hamiltonian. The latter fact might complicate the comparison to other techniques.

Using the temperature-flow RG scheme, we have analyzed the flow to strong coupling for the two-dimensional  $t$ - $t'$  repulsive Hubbard model on the square lattice. The results obtained agree qualitatively with a various other calculations.

The flow to strong coupling in the parameter region of small next nearest neighbor hopping  $t'$  shows strong similarities to the RG flow known from the momentum-shell techniques<sup>11,14,15</sup>. Again AF and  $d$ -wave tendencies are coupled to a large extent and the FS curvature determines which of the two types of fluctuations is strongest: when we move

away from perfect nesting, the AF processes are cut off at low temperatures and the  $d_{x^2-y^2}$ -wave Cooper scattering processes can diverge.

For larger absolute values of  $t'$  beyond a critical  $t'_c \approx -0.33t$  we find that the flow to strong coupling is dominated by ferromagnetic fluctuations. This regime has not been found with the momentum-shell schemes used recently<sup>11,14,15</sup> for the reasons explained in the introduction.

There are several other approaches which predict ferromagnetic ground states for larger  $|t'|$ . Lin and Hirsch<sup>23</sup> analyzed the Hartree-Fock phase diagram for the  $t$ - $t'$  Hubbard model and found the ferromagnetic state to be stable against the antiferromagnetic state for  $t' < -0.324t$ . They do not find a  $d$ -wave phase for  $t' > -0.324t$  because the bare repulsive Hubbard interaction does not contain any attractive component in the pair scattering channel. The critical  $t'$ -value from Hartree-Fock is practically equivalent to the critical  $t'_c \approx -0.33t$  from the RG treatment. On the other hand in Hartree-Fock one would find a first order transition at  $t'_c$ , while in our treatment the characteristic temperature gets suppressed to zero at the quantum critical point. Irkhin et al.<sup>27</sup> applied a parquet scheme using the same set of one-loop diagrams as the RG described above. With a simplified dispersion they found indications for ferromagnetism close to  $t' = -0.5t$  and emphasized the strong deviations of the critical temperatures from the simple Stoner calculation. Hlubina et al.<sup>24,25</sup> analyzed the question of ferromagnetism by applying quantum Montecarlo and T-matrix approximation (TMA). The latter method gave a ferromagnetic state beyond a critical  $t' \approx -0.43t$ . The Kanamori-screening in the particle-particle channel of the TMA is included in our temperature-flow scheme, which gives a larger window for a ferromagnetic ground state. This suggests that the straightforward TMA might overestimate the screening effects in the given example. We repeat however that defining the initial condition for two-point and four-point vertex functions in the temperature-flow RG is not fully equivalent to using a specific microscopic Hamiltonian in the perturbative scheme. Arachea<sup>40</sup> found spin-polarized ground states in exact diagonalization studies of a  $4 \times 4$   $t$ - $t'$  cluster for  $t' = -0.4t$  and  $t' = -0.6t$  at densities 0.5 and 0.375.

For several classes of models<sup>18-20,22</sup> large-spin ground states can be proved exactly. Among those, the so-called flat band ferromagnetism appears to have the closest relation to the case of the  $t$ - $t'$  Hubbard model. The typical feature of these models is a large density of states at the bottom of the band which gets pushed further below the Fermi energy by polarizing the system. In the 2D  $t$ - $t'$  Hubbard model for  $t' \rightarrow -0.5t$  the density of states is peaked at the bottom of the band. Nonetheless from the perspective of our RG calculation the large density of states at the FS appears to be essential for the FM tendencies in the  $t$ - $t'$  Hubbard model, as the latter are strongly reduced when one raises the Fermi level above the van Hove energy. Moreover, if we cut out the bottom of the band by hand and discard all modes with  $\epsilon_{\vec{k}} < -0.1t$ , the ferromagnetic tendencies do increase rather than decrease, presumably due to the reduced screening of the onsite repulsion. Thus the peak at the bottom of the band is not essential for our finding of ferromagnetic tendencies. The sensitivity of the ferromagnetic regime to the location of the FS points to another effect which is not included in the present calculation. It is probable that the inclusion of selfenergy effects in the flow will shift the Fermi surface and alter the low energy density of states such that the actual ferromagnetic regime might be changed. A calculation of the selfenergy at the FS from the flow of the interactions shows however that the real part of the selfenergy becomes comparable to the temperature only when the couplings have grown larger than the bandwidth to  $V_{T,\max.} \approx 12 - 13t$ .

In analogy with the interplay between AF and  $d$ -wave fluctuations close to perfect nesting at smaller  $t'$ , there exists a parameter region for larger  $|t'|$  where the FM tendencies get cut off and the flow to strong coupling is dominated by  $p_x$ - and  $p_y$ -wave superconducting correlations. The energy gap suggested by the RG flow of the Cooper pair scattering is highly anisotropic and exhibits minima on the FS parts close to the saddle points. Similar scenarios have already been proposed by several authors<sup>24,25,41</sup>, our approach allows a more systematic analysis of the crossover from the FM to  $p$ -wave regime and the possible order parameter symmetries. We note that the superconducting gap functions suggested by the RG flow  $\propto p_x + ip_y$  are among the candidates under debate for the superconducting state of  $\text{Sr}_2\text{RuO}_4$ <sup>42</sup>. In this quasi-two-dimensional system one of the three Fermi surfaces has a similar shape as the cases studied above. It should be interesting to investigate the RG flow and the superconducting properties suggested by the resulting pair scattering in a more realistic three-band model.

Another future application of the modified RG scheme could be to investigate the interplay of screening of long-range forces with other tendencies. Further, other potential instabilities in forward-scattering channel could be analyzed, e.g. Labbe-Friedel or Pomeranchuk instabilities with spontaneous deformations of the FS, as proposed by Halboth and Metzner<sup>14</sup>.

We are grateful to T.M. Rice, M. Sigrist, R. Hlubina, P. Monthoux, M.E. Zhitomirsky and D. Vollhardt for valuable discussions. C.H. acknowledges financial support through the Swiss National Science Foundation.

- <sup>1</sup> M.Salmhofer, *Renormalization: An Introduction*, Texts and Monographs in Physics, Springer (1999), and references therein.
- <sup>2</sup> R.Shankar, Rev. Mod. Phys. **66**, 129 (1994).
- <sup>3</sup> T. Chen, J. Fröhlich, and M. Seifert, cond-mat/9508063, appeared in *Fluctuating Geometries in Statistical Mechanics and Field Theory*, edited by F. David, P. Ginsparg, and J. Zinn-Justin, Elsevier Science B.V. (1996); see also J. Fröhlich and R. Götschmann, Phys. Rev. **B55**, 6788 (1996).
- <sup>4</sup> For a review, see: J. Solyom, Adv.Phys. **28**, 201 (1979).
- <sup>5</sup> V. J. Emery, *Highly Conducting One-Dimensional Solids*, ed. J.T. Devreese, R. E. Evrar, and V.E. van Doren, Plenum, New York (1979).
- <sup>6</sup> J. Voit, Rep. Prog. Phys. **57**, 977 (1994).
- <sup>7</sup> I. Dzyaloshinskii, Sov.Phys.JETP **66**, 848 (1987); I. Dzyaloshinskii, J.Phys.I (France) **6**, 119 (1996).
- <sup>8</sup> H.J. Schulz, Europhys.Lett. **4**, 609 (1987).
- <sup>9</sup> P. Lederer, G. Montambaux and D. Poilblanc, J.Phys. **48**, 1613 (1987).
- <sup>10</sup> J. Gonzales et al., Europhys.Lett. **34**, 711 (1996); J. Gonzales et al., Nuc.Phys. B **485**, 694 (1997).
- <sup>11</sup> D. Zanchi and H.J. Schulz, Europhys.Lett. **44**, 235 (1997); D. Zanchi and H.J. Schulz, Phys.Rev. B **61**, 13609 (2000)
- <sup>12</sup> J.V. Alvarez et al., J.Phys.Soc.Jpn. **67**, 1868 (1998).
- <sup>13</sup> N. Furukawa, T.M. Rice, and M. Salmhofer, Phys.Rev.Lett. **81**, 3195 (1998).
- <sup>14</sup> C.J. Halboth and W. Metzner, Phys.Rev. B **61**, 7364 (2000); Phys. Rev. Lett. **85**, 5162 (2000).
- <sup>15</sup> C. Honerkamp, M. Salmhofer, N. Furukawa, and T.M. Rice, Phys. Rev. B **63** (2001).
- <sup>16</sup> C. Honerkamp, to appear in Euro. Phys. J. B (2000).
- <sup>17</sup> K. Yosida, *Theory of Magnetism*, Springer Series in Solid State Sciences 122, Springer, Berlin (1996).
- <sup>18</sup> P. Fazekas, *Lecture Notes on Electron Correlation and Magnetism*, World Scientific, Singapore (1999).
- <sup>19</sup> H.Tasaki, Prog. Theor. Phys. **99**, 489 (1998).
- <sup>20</sup> A. Mielke, Phys. Rev. Lett. **82**, 4312 (1999), J. Phys. A, Math. Gen. **32**, 8411 (1999).
- <sup>21</sup> M. Ulmke, Euro. Phys. J. B **1**, 301 (1998).
- <sup>22</sup> D. Vollhardt, N. Blümer, K. Held, and M. Kollar, cond-mat/0012203; D.Vollhardt, N.Blümer, K.Held, M.Kollar, J.Schlipf, M.Ulmke, and J.Wahle, *Advances in Solid State Physics* **38**, 383 (1999).
- <sup>23</sup> H.Q. Lin and J.E. Hirsch, Phys. Rev. B **35**, 3359 (1987).
- <sup>24</sup> R. Hlubina, S. Sorella, and F. Guinea, Phys. Rev. Lett. **78**, 1343 (1997).
- <sup>25</sup> R. Hlubina, Phys. Rev. B **59**, 9600 (1999).
- <sup>26</sup> M. Fleck, A. Oles, and L. Hedin, Phys. Rev. B **56**, 3159 (1997).
- <sup>27</sup> V.Yu. Irkhin, A.A. Katanin, and M.I. Katsnelson, cond-mat/0102381.
- <sup>28</sup> This also applies to the modified one-loop scheme proposed recently by Kopietz and Busche<sup>29</sup>.
- <sup>29</sup> P. Kopietz and T. Busche, cond-mat/0103633.
- <sup>30</sup> J. Kanamori, Prog. Theo. Phys. **30**, 275 (1963).
- <sup>31</sup> Related effects in the flow of the forward scattering amplitudes have also been analyzed by Metzner et al.<sup>32</sup>.
- <sup>32</sup> W. Metzner, C. Castellani, and C. Di Castro, Adv. Phys. **47**, 317 (1998).
- <sup>33</sup> This is in contrast with the expressions used by Alvarez et al.<sup>12</sup> in their scaling treatment of the saddle point regions. These authors claim a logarithmic cutoff-dependence of the particle-hole bubble with zero momentum transfer which then generates ferromagnetic correlations at finite RG scale.
- <sup>34</sup> M.Salmhofer and C.Honerkamp, Prog. Theo. Physics **105**, 1 (2001).
- <sup>35</sup> A.L. Fetter, J.D. Walecka, *Quantum Theory of Many-Particle Systems*, Mc Graw-Hill, New York (1971).
- <sup>36</sup> A flow where the particle number is fixed instead of  $\mu$  gives qualitatively similar results. The same holds for smaller initial interactions, e.g.  $U = 2.5t$ .
- <sup>37</sup>  $U\chi_s^0(\vec{q}, T_c) = -1$  with  $\vec{q} = (\pi, \pi)$  for  $t' \rightarrow 0$  or  $\vec{q} = 0$  for  $t' \rightarrow -0.5t$ , see e.g. Ref. 18.
- <sup>38</sup> T.M. Rice and M. Sigrist, J. Phys. Cond. Mat. **7**, L643 (1995).
- <sup>39</sup> K.K. Ng and M. Sigrist, Europhys. Lett. **49**, 473 (2000).
- <sup>40</sup> L. Arachea, Phys. Rev. B **62**, 10033 (2000).
- <sup>41</sup> J. Gonzalez, F. Guinea, and M.A.H. Vozmediano, Phys.Rev. Lett. **84**, 4930 (2000).
- <sup>42</sup> For review see Y. Maeno, T.M. Rice, and M. Sigrist, Physics Today **54**, 42 (2001).